











Atomic ordering and bond relaxation in optical spectra of self-organized InP/GaInP₂ Wigner molecule structures

Cite as: Appl. Phys. Lett. **115**, 202104 (2019); <https://doi.org/10.1063/1.5126527>

Submitted: 03 September 2019 . Accepted: 24 October 2019 . Published Online: 12 November 2019

A. M. Mintairov , D. V. Lebedev, N. Bert , K. G. Belyaev, V. N. Nevedomskiy, M. V. Rakhlin , A. A. Toropov , A. S. Vlasov , A. Gocalinska , G. Juska , E. Pelucchi , M. A. Arredondo, A. B. Naden , A. V. Shelaev , and V. A. Bykov



View Online



Export Citation



CrossMark

ARTICLES YOU MAY BE INTERESTED IN

[Suppression of substrate coupling in GaN high electron mobility transistors \(HEMTs\) by hole injection from the p-GaN gate](#)

Applied Physics Letters **115**, 203502 (2019); <https://doi.org/10.1063/1.5121637>

[Unusual electric field-induced optical behaviors in cesium lead bromide perovskites](#)

Applied Physics Letters **115**, 201101 (2019); <https://doi.org/10.1063/1.5116326>

[Strain-driven lattice distortion and the resultant magnetic properties of La_{0.7}Sr_{0.3}MnO₃/BaTiO₃ superlattices](#)

Applied Physics Letters **115**, 201604 (2019); <https://doi.org/10.1063/1.5119736>

Lock-in Amplifiers
... and more, from DC to 600 MHz



Atomic ordering and bond relaxation in optical spectra of self-organized InP/GaInP₂ Wigner molecule structures

Cite as: Appl. Phys. Lett. **115**, 202104 (2019); doi: 10.1063/1.5126527

Submitted: 3 September 2019 · Accepted: 24 October 2019 ·

Published Online: 12 November 2019

















View Online



Export Citation



CrossMark

A. M. Mintairov,^{1,2,a)}  D. V. Lebedev,¹  N. Bert,¹  K. G. Belyaev,¹  V. N. Nevedomskiy,¹  M. V. Rakhlin,¹  A. A. Toropov,¹  A. S. Vlasov,¹  A. Gocalinska,³  G. Juska,³  E. Pelucchi,³  M. A. Arredondo,⁴  A. B. Naden,^{4,5}  A. V. Shelaev,⁶  and V. A. Bykov⁶

AFFILIATIONS

¹Ioffe Institute, Saint Petersburg, 194021, Russia

²Electrical Engineering Department, University of Notre Dame, Notre Dame, Indiana 46556, USA

³Tyndall National Institute, University College Cork, Cork, T12R5CP, Ireland

⁴School of Mathematics and Physics, Queen's University Belfast, Belfast, BT7 1NN, United Kingdom

⁵School of Chemistry, University of St Andrews, St Andrews, KY16 9ST, United Kingdom

⁶NT-MDT Co, Zelenograd, Moscow 124460, Russia

a)amintairov@gmail.com

ABSTRACT

We used transmission electron microscopy, Raman, and photoluminescence spectroscopy to identify the effect of CuPt-type GaP-InP atomic ordering (AO) on the structural and emission properties of self-organized (SO) InP/GaInP₂ Wigner molecule (WM) quantum dot (QD) structures. We found that the correlation of AO and SO growth results in the formation of InP/GaInP₂ QD/AO-domain (QD/AOD) core-shell composites. This observation shows that intrinsic WMs in this system emerge due to a strong piezoelectric field generated by AODs, which induces QD doping and a built-in magnetic field. We found that the bond relaxation of AODs leads to a decrease in the emission energy of WMs of 80 meV. The photoluminescence spectra of single WMs having an emission energy ~ 1.53 eV are presented here, the lowest one reported for this system.

© 2019 Author(s). All article content, except where otherwise noted, is licensed under a Creative Commons Attribution (CC BY) license (<http://creativecommons.org/licenses/by/4.0/>). <https://doi.org/10.1063/1.5126527>

Among a variety of self-organized (SO) semiconductor quantum dot (QD) systems realized to date, which include III-V, II-VI, and III-N (nitride) materials,¹ phosphide III-V QDs grown on GaAs substrates are the only ones which can provide a weak quantum confinement and accumulation of up to 20 electrons *in situ*^{2,3} similar to that realized in electrostatically controlled, nanofabricated QDs.^{4,5} Moreover, strong built-in magnetic fields^{6,7} can exist in these QDs, creating a quantum Hall regime at a zero external magnetic field. Thus, these QDs represent natural two-dimensional electron/quantum Hall puddles and/or electron/composite fermion⁸ Wigner molecules (WMs)⁹ and are interesting for fundamental and applied research in quantum physics, nanoelectronics, and conventional⁵ and fault tolerant topologically protected¹⁰ quantum computing. Moreover, due to a very strong photoluminescence (PL) intensity and efficient cavity-mode-QD coupling, these WM QDs provide the

lowest lasing threshold of optical microresonators¹¹ and are interesting for nanophotonic applications.

These natural WM structures are n-type lens shape InP islands obtained using SO metal-organic vapor phase epitaxy (MOVPE) by the deposition of few monolayers (MLs) of InP on Ga_{0.51}In_{0.49}P, or, simply, GaInP₂, lattice-matched to GaAs. The islands have a lateral size 80–180 nm, height 5–25 nm, Ga content 0–0.25, and density 2–10 μm^{-2} . It was found that optimal SO InP/GaInP₂ WM QD structures, in terms of the electron occupation, size distribution, and density, are obtained using a substrate having a nearly exact [001] orientation or 2° misorientation toward the [110] direction, deposition of 3 ML of InP, growth temperature $T_g = 720^\circ$, and a III-V ratio of 120, as reported previously.⁹

An intrinsic property of GaInP₂ lattice-matched to GaAs is atomic ordering (AO),^{12,13} which appears as a GaP-InP monolayer

superlattice along one of the two $\langle 111 \rangle_B$ zinc blende diagonals, known as the CuPt_B-type crystal structure. In epitaxial GaInP₂ films, this is represented by the $[1\bar{1}1]$ or $[11\bar{1}]$ oriented AO domains (AODs) and antiphase boundaries having a size of 5–500 and 1–40 nm and occupying up to 50% and 10% of the material volume, respectively, depending on the growth conditions.^{14–16} A strong AO (i.e., large and dense AODs) lowers the bandgap of GaInP₂ by up to 150 meV,¹⁷ generates a piezoelectric field of up to ~ 200 kV/cm,¹⁸ and creates a symmetry misfit strain.¹⁹ The AODs can be strained or relaxed, i.e., have GaAs cubic or $[111]$ -GaP/InP rhombohedral in-plane atom positions.¹⁹ Thus, AO can strongly affect doping, confinement potential, optical properties, and formation of WMs; however, previous reports on the growth of InP/GaInP₂ structures^{2,9} did not consider this effect. On the other hand, the growth of InP QDs should affect AO and it was found that ordered GaInP₂ islands can be formed on top of SO InP QDs grown at 580 °C.²⁰

Here, we used transmission electron microscopy (TEM), Raman, and temperature dependent μ -PL spectroscopy measurements, including near-field scanning PL, to study the effect of CuPt_B-type AODs on the structural and emission properties of InP/GaInP₂ SO QD structures grown by low pressure MOVPE.²¹ Using cross section TEM imaging to monitor the location of AODs, we report the formation of InP/GaInP₂ QD/AOD core-shell composites consisting of an InP QD core surrounded by a few GaInP₂ AODs having a lateral size and height of 20–50 and 2–15 nm, respectively. By low-temperature μ -PL spectra, we observed a set of narrow emission lines and peaks in the range 1.92–1.52 eV. In this set, we identified QD-type excitonic lines related to GaInP₂ AODs, and excitonic/WM lines/peaks related to coherent and incoherent InP QDs. We found an 80 meV decrease in the emission energy of the WM QDs due to the bond relaxation (BR) of AODs and we demonstrate that the emission spectra of single WMs can have an emission energy as low as 1.53–1.55 eV.

The QD WM structure discussed here, sample number A2389 and henceforth denoted as R1, was grown using the following conditions: $T_g = 680$ °C, III-V ratio 400, and substrate misorientation (SM) 0.2° toward $[111]_A$. This growth differs from the somehow optimal conditions described in Ref. 9. Thus, the data for R1 were compared with sample AIX2421 (denoted as U2 from this point forward), which was grown under the conditions described in Ref. 9. Furthermore, the PL spectra of these samples were compared with sample ii from Ref. 2, grown at lower T_g (650 °C) and with a thicker InP deposition (8 ML), denoted here as U0.

Raman spectra were excited by the 532 nm line of a solid-state laser from the (001) plane and measured in the backscattering geometry using a CCD and a 0.5 m focal length spectrometer in two parallel configurations (XX) and (YY), where $X||[1\bar{1}0]$ and $Y||[110]$. We should point out that the Raman technique is the only one we can think of as capable of addressing the strain/relaxation status of AODs. Plan-view TEM samples were prepared by conventional mechanical polishing using a Gatan simplifier grinder, followed by Ar⁺ milling in a PIPSII. Cross section TEM samples were prepared through a conventional mechanical polishing using a Model 590 Tripod Polisher followed by Ar⁺ milling in a PIPS 691. TEM specimens were characterized using a JEOL 2100F and an FEI G2 Talos microscopes operating at an accelerating voltage of 200 kV. μ -PL measurements were conducted at different temperatures in the range 10–300 K. Single dot measurements were performed using ozone plasma

treatment, quenching the emission of the major part of the dots. The full details of room temperature near-field scanning optical microscopy (NSOM) and ensemble/single dot μ -PL spectroscopy are described in Ref. 9.

In Raman spectra [see Fig. 1(a)], we observed the difference in the intensity of the (XX) and (YY) configurations for the GaP-type longitudinal phonon (LO₁) at 382 cm⁻¹ and an antiphase boundary vibrational mode (Y') at 355 cm⁻¹ in both R1 and U2 samples, which are the signatures of AO in GaInP₂ layers.¹⁹ In the R1 sample, the LO₁ phonon has a stronger intensity in the (XX) configuration indicating the relaxation of AODs [see the inset in Fig. 1(a)]. The LO₁ phonon in the U2 sample has two components: one, near 379 cm⁻¹, which is stronger in the (XX) configuration and similar to that of R1, and the other, near 383 cm⁻¹, which is stronger in the (YY) configuration, indicating unrelaxed (strained) AODs. BR gives a mismatch of -1.5% for the $[1\bar{1}0]$ direction and +1.7% for the $[110]$ direction corresponding to the frustration of Ga-P and the compression of In-P bonds. Thus, changing the SM, T_g , and III-V ratio results in the switching between the unrelaxed and relaxed states of AODs.

Selected area electron diffraction (SAED) of sample R1 in Fig. 2(a) reveals the superstructure reflections along with the fundamental zinc blende spots. The $[\bar{1}10]$ -pole SAED pattern contains superlattice spots at $1/2\{111\}$ with a pronounced streaking along the $[001]$ axes which are typical features of CuPt-type ordering on both (111) and ($\bar{1}\bar{1}\bar{1}$) planes.^{12,13} Therefore, two types of domains with ordering on two mirror $\{111\}$ planes and antiphase boundaries are present, confirming the Raman observations of the AO. Similar SAED patterns indicating the AO were obtained for U2, U0, and other samples.

The 002 dark-field (DF) cross section images clearly revealed the InP QDs as nanometer-sized islands within the 140 nm thick GaInP₂ film. Most islands were observed to be flat with $h = 3$ –5 nm, lateral dimensions of 100–150 nm, and a density of approximately 50 μm^{-2} . These are type A QDs (see Ref. 2). Among them, thicker quantum dots having $h \sim 20$ nm (type B QDs) rarely occur. We also observed a few defected regions having sizes of ~ 150 nm and $h \sim 40$ nm, which can be attributed to C-type dots.² An example of a 002 DF cross

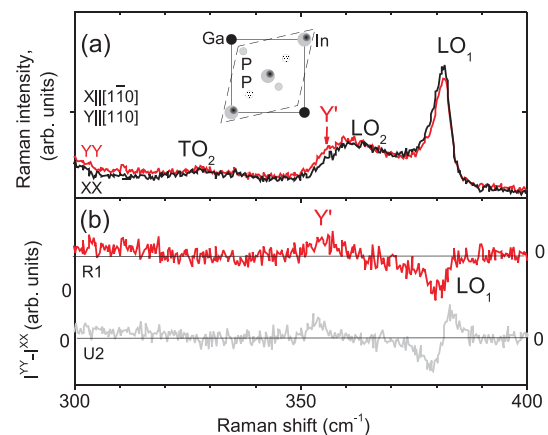


FIG. 1. Raman spectra of sample R1 measured in backscattering configurations XX and YY—(a) and comparison of (YY)-(XX) difference spectra of samples R1 and U2. Inset—strained arrangement of Ga, In, and P atoms in the (001) plane (the dashed lines show distortion due to bond relaxation, i.e., CuPt-type bond lengths).

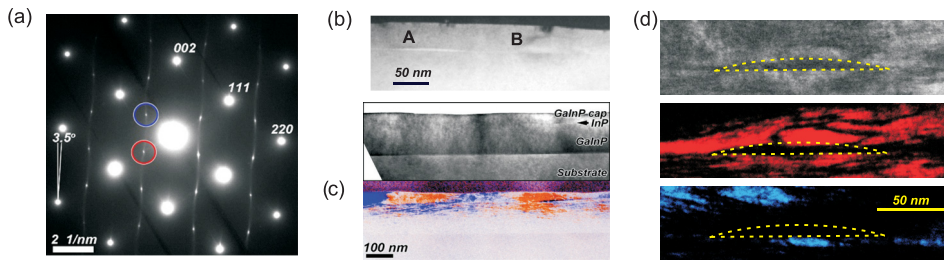


FIG. 2. $[\bar{1}10]$ -pole electron diffraction pattern of sample R1-(a); 002 dark-field cross section image (b); $[\bar{1}10]$ -zone bright-field TEM micrograph of the sample R1 (c and d—top), a combined picture comprising two overlaid (c—bottom) or separated (d—middle and bottom) dark-field micrographs taken with $\frac{1}{2}(111)$ and $\frac{1}{2}(\bar{1}\bar{1}\bar{1})$ extra-reflections (circled in a) from the same region of the sample. The dashed lenticular shape in d outlines the QD.

section image showing one A- and one B type QD is represented in Fig. 2(b).

The upper part of Fig. 2(c) provides a $[\bar{1}10]$ -zone bright-field (BF) micrograph showing the general view of $\sim 1 \mu\text{m}$ area of the GaInP₂ epitaxial layer. In the bottom part of Fig. 2(c), a combination of two overlaid DF micrographs taken with $\frac{1}{2}(111)$ and $\frac{1}{2}(\bar{1}\bar{1}\bar{1})$ extra-reflections from the same region of the sample is presented. The overlaid micrographs are false-colored; the AODs having the $[\bar{1}\bar{1}\bar{1}]$ or $[\bar{1}11]$ direction are shown in blue and red, respectively. The domains at the bottom of the GaInP₂ layer are seen as lamellae with a lateral size of 10–100 nm and a thickness of a few nm. The domains in the cap GaInP₂ layer become thicker and occupy the whole 40–50 nm thick cap, with their lateral size being 150–200 nm.

In the upper image of Fig. 2(d), we show the 200 nm area $[\bar{1}10]$ -zone BF TEM micrograph of an InP QD having a lateral size of 110 nm and a height of 9 nm, appearing as a dark lenticular island. In the same region, AODs with $[\bar{1}\bar{1}\bar{1}]$ or $[\bar{1}11]$ directions are marked with a red and blue contrast in the central and bottom parts of Fig. 2(d), respectively. We observed one $[\bar{1}\bar{1}\bar{1}]$ and three $[\bar{1}\bar{1}\bar{1}]$ AODs having a lateral size of ~ 20 nm, adjacent to the bottom, as well as two large (~ 50 nm) and one small (~ 15 nm) $[\bar{1}\bar{1}\bar{1}]$ AODs adjacent to the top of the QD. Thus, the full structure of the QD is characterized as an InP/GaInP₂ QD/AOD core-shell composite. This indicates a correlation between the AO and SO growth, which agrees with the observation in Ref. 20. We should point out that in the upper image in Fig. 2(d), there are light-gray areas coinciding with AODs. Thus, the total height of the composite is ~ 20 nm, which could indicate that B-type dots are represented by these composites.

AODs generate a strong piezoelectric field of ~ 200 kV/cm along the $[\bar{1}\bar{1}\bar{1}]$ or $[\bar{1}11]$ directions¹⁸ resulting in QD doping, as it is well known in GaN/AlN structures,²² and leading to the formation of WMs. The in-plane inhomogeneity of this field can generate a build-in magnetic field. Thus, the formation of the QD/AOD composite is a key feature for the existence of natural InP/GaInP₂ WMs.

In the plan-view TEM image [see Fig. 3(a)], the InP QDs appear as gray and dark-gray spots having a size of 80–120 and 150–200 nm, and a density of $\sim 2 \mu\text{m}^{-2}$ for both sizes, respectively. We attribute the changes in the gray contrast to the changes in the dot thickness and, accounting for the small density observed, we assign these to B- and C-type dots, respectively. A-type dots are not observed in the plan-view due to their small height. C-type dots, having a size >150 nm, show defect boundaries, suggesting incoherent relaxation of strain, as observed in the cross section TEM.

Figure 3(b) shows the NSOM images acquired at a power density of 50 kW/cm^2 with spectral ranges of 740–780 and 640–680 nm, related to the ranges of InP QD and GaInP₂ emission, respectively [see the single dot NSOM PL spectrum in the inset in the upper part of Fig. 3(b)]. In the image taken for the 740–800 nm range, the QDs appear as bright spots having a density of $\sim 2 \mu\text{m}^{-2}$, i.e., the same as in the plan-view TEM image in Fig. 3(a). The size of the emission area (dashed circles) estimated from the image is ~ 90 nm and thus, they are related to B-type dots. On the other hand, in the image taken for the 640–680 nm range, the QDs appear as dark-gray and gray spots, which arise due to the absorption of GaInP₂ emission by the QD material. The gray spots are related to B-type dots and their position coincides with the position of bright spots of the QD emission image. The size estimated from the absorption profile is ~ 120 nm, and is larger than the emission area due to the partial filling of QD states by the photoexcited carriers involved in the emission process. At the same time, the absorption images of B-type dots show a slight decrease in the absorption at the center, due to band filling, i.e., bleaching. The dark-gray spots have sizes of 150–200 nm and are related to C-dots. These appeared dark at room temperature due to nonradiating defects.

The lateral size probability distribution function (PDF) of the sample R1 has two maxima, at 85 and 150 nm, having a FWHM of ~ 40 nm [see Fig. 3(c)]. While, the sample U2 has its maxima at larger sizes, 130 and 170 nm, which indicates a decrease in the adatoms'

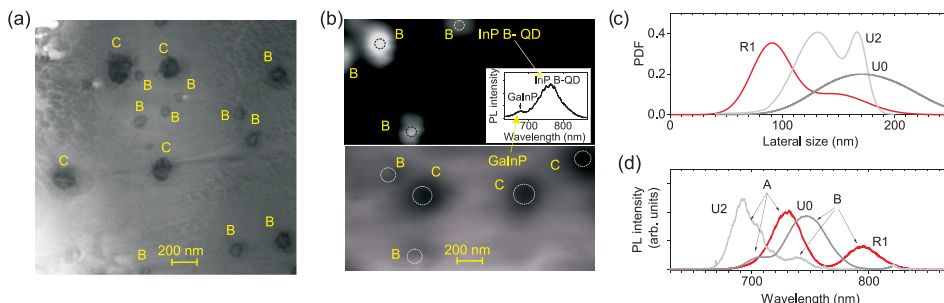


FIG. 3. Plan-view TEM (a) and NSOM (b) images of sample R1; comparison of the lateral size probability distribution function (c) and 77K spectrum (d) of samples R1 and U2. The inset in (b) shows the NSOM PL spectra of individual QD and NSOM images, which were taken at wavelength ranges 720–820 (upper) and 640–680 nm (lower) of the same area. The dashed circles in (b) show the QD size estimated from the images.

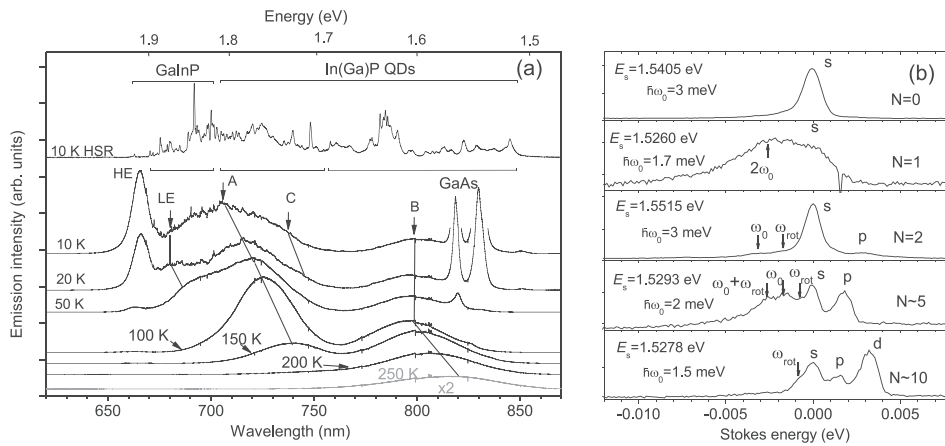


FIG. 4. Temperature dependent ensemble (a) and single WM 10 K- μ -PL (b) spectra of InP/GaInP₂ sample R1. WM spectra plotted vs Stokes energy.

diffusion length for [111]_A SM. For sample U0, the PDF has one maximum at 180 nm and a large FWHM of ~ 100 nm, which is due to Ostwald ripening.²

The comparison of the 77 K PL spectra for R1, U2, and U0 samples shows an increase in the emission wavelength of InP QDs due to the BR of AODs. For sample R1, the A- and B-type dots were found to have an emission wavelength of ~ 720 and 800 nm, while for samples U2 and U0, the dots have an emission wavelength of 700–710 and 730–750 nm, respectively. In sample U0, the emission bands overlap with the bands of sample R1, indicating some fraction of relaxed AODs. Moreover, the Raman spectra in Fig. 1(b) indicate the existence of some fraction of relaxed AODs in the U2 sample. For unrelaxed AODs, the emission energy of InP QDs, neglecting In-Ga intermixing, is 1.61 eV,² which has a ~ 200 meV blue shift compared to bulk InP due to the strain arising from the 3.8% lattice mismatch with GaInP₂. For relaxed AO GaInP₂, the decrease in the emission energy is 80 meV, i.e., ~ 0.4 of total shifts. This value agrees very well with the 0.4 change of the lattice mismatch due to BR.

In the ensemble μ -PL spectra of sample R1 measured at temperatures $T = 250, 200, 150, 100, 50, 20,$ and 10 K, [see Fig. 4(a)] only the band related to the B-type dots is observed for $T = 200$ –300 K. At $T = 250$ K, it has a maximum at 820 nm and an FWHM of ~ 30 nm. At $T = 150$ K, another band having an FWHM of ~ 30 nm related to A-type dots appears at 740 nm. When the temperature further decreases, the A-band shifts to lower wavelengths reaching ~ 700 nm at 10 K. It starts revealing a fine structure at 20 K. At $T = 50$ K, a shoulder of the A-band related to C-dots appears at 740 nm and two shoulders related to the HE and LE bands of AO GaInP₂, reported previously,^{23–25} appear at 650 and 685 nm, respectively. The LE band reveals a fine structure at $T = 20$ K. Also at 20 K, two GaAs substrate peaks having an FWHM of ~ 5 nm appear at 820 and 830 nm. We should point out that the wide spectral range (50–90 nm) of the emission of A- and B-type InP QDs indicates Ga-In intermixing,² which can reach values up to 0.25 and thus the emission at lower wavelengths of these ranges originates from In(Ga)P QDs.

In the 10 K μ -PL spectra of the specimen having a reduced dot density, all bands, except HE, decay on sharp emission lines (FWHM < 1 meV). This is related to QD-type excitonic transitions of the AODs of GaInP₂^{26,27} and InP and In(Ga)P QDs, as well as broader peaks (FWHM ~ 1 –5 meV) related to InP and In(Ga)P WMs.

In Fig. 4(b), we show a set of selected single dot spectra of five B-type dots having emission energies of 1.53 to 1.55 eV and different electron occupancies (N). One dot has $N = 0$ and shows a single s emission exciton peak. While, the rest of the dots are WMs, having $N = 1$ –10 and $\hbar\omega_0 = 1.5$ –3 meV, revealing the features previously reported for unrelaxed AO WMs having emission energies of 1.7–1.8 eV.⁹ For $N = 1$, the spectrum has a broad Stokes feature indicating a formation of 2 electrons ($2e$) WM in the photoexcited state; for $N = 2$ and 5, anti-Stokes peaks related to the p electrons of $3e$ - and $6e$ -WMs in the photoexcited state, and Stokes peaks related to rotational (ω_{rot}) and translational (ω_0) modes of $2e$ - and $5e$ -WMs in the initial states, are observed; for $N \sim 10$, an additional anti-Stokes peak related to the d electrons of $11e$ -WM appears.⁹

In conclusion, we report the effect of CuPt_B-type AO on the structural and emission properties of InP/GaInP₂ SO WM QDs. We observed the formation of InP/GaInP₂ QD/AOD core-shell composites and found that AQDs can be relaxed. In low-temperature μ -PL spectra, we observed a set of emission lines related to the excitons of QD-like GaInP₂ AODs and the excitons/WMs of coherent and incoherent InP QDs. The PL spectra of single WMs having a number of electrons $N = 2$ –10, quantum confinement $\hbar\omega_0 = 1.5$ –3 meV, and emission energy as low as 1.53 eV, resulting from AOD BR, were identified in the μ -PL spectra. Our observations elucidate the existence of natural WM as a result of the correlation of AO and SO growth and the strong piezoelectric fields generated by AODs.

A.M.M., D.V.L., and A.S.V. acknowledge the support of the Russian Science Foundation Grant No. 19-19-00246. K.G.B., M.V.R., and A.A.T. acknowledge the financial support of the Russian Foundation for Basic Research (Project No. 18-02-01212). This research was also enabled by the Science Foundation Ireland under Grant Nos. 15/IA/2864, 12/RC/2276, 12/RC/2276-P2, and 18/US/3512, and the Northern Ireland Department for the Economy (Grant No. USI-140). A.B.N. acknowledges support from EPSRC grant no. EP/R023751/1.

REFERENCES

- E. Michler, *Single Semiconductor Quantum Dots* (Springer, Berlin/Heidelberg, 2009), p. 390; Z. M. Wang, *Self-Assembled Quantum Dots* (Springer Berlin/Heidelberg, 2008), p. 468.

- ²J. Kapaldo, S. Rouvimov, J. L. Merz, S. Oktyabrsky, S. A. Blundell, N. Bert, P. Brunkov, N. A. Kalyuzhnyy, S. A. Mintairov, S. Nekrasov *et al.*, *J. Phys. D: Appl. Phys.* **49**, 475301 (2016).
- ³A. M. Mintairov, J. Kapaldo, J. L. Merz, A. S. Vlasov, and S. A. Blundell, *Phys. Rev. B* **95**, 115442 (2017).
- ⁴L. P. Kouwenhoven, D. G. Austing, and S. Tarucha, *Rep. Prog. Phys.* **64**, 701 (2001).
- ⁵R. Hanson, L. P. Kouwenhoven, J. R. Petta, S. Tarucha, and L. M. K. Vandersypen, *Rev. Mod. Phys.* **79**, 1217 (2007).
- ⁶A. M. Mintairov, N. A. Kalugnyy, V. M. Lantratov, S. A. Mintairov, and J. L. Merz, *J. Phys.: Conf. Ser.* **245**, 012041 (2010).
- ⁷A. M. Mintairov, J. L. Merz, and S. Blundell, "Molecular states of electrons: Emission of single molecules in self-organized InP/GaInP quantum dots," in *Fingerprints in the Optical and Transport Properties of Quantum Dots* (InTech, 2012), p. 468.
- ⁸J. K. Jain and T. Kawamura, *Europhys. Lett.* **29**, 321 (1995).
- ⁹A. M. Mintairov, J. Kapaldo, J. L. Merz, S. Rouvimov, D. V. Lebedev, N. A. Kalyuzhnyy, S. A. Mintairov, K. G. Belyaev, M. V. Rakhlin, A. A. Toropov *et al.*, *Phys. Rev. B* **97**, 195443 (2018).
- ¹⁰S. D. Sarma, M. Freedman, and C. Nayak, *Phys. Rev Lett.* **94**, 166802 (2005).
- ¹¹Y. Chu, A. M. Mintairov, Y. He, J. L. Merz, N. A. Kalugnyy, V. M. Lantratov, and S. A. Mintairov, *Phys. Status Solidi C* **8**, 325 (2011).
- ¹²P. Bellon, J. P. Chevalier, G. P. Martin, E. Dupont Nivet, C. Thiebaut, and J. P. André, *Appl. Phys. Lett.* **52**, 567 (1988).
- ¹³A. Gomyo, T. Suzuki, and S. Iijima, *Phys. Rev. Lett.* **60**, 2645 (1988).
- ¹⁴E. Morita, M. Ikeda, O. Kumagai, and K. Kaneko, *Appl. Phys. Lett.* **53**, 2164 (1988).
- ¹⁵P. Bellon, J. P. Chevalier, E. Augarde, J. P. André, and G. P. Martin, *J. Appl. Phys.* **66**, 2388 (1989).
- ¹⁶A. Mascarenhas, *Spontaneous Ordering in Semiconductor Alloys* (Springer Science+Business Media LLC, New York, 2002), p. 474.
- ¹⁷M. Schubert, B. Rheinlander, and V. Gottschalch, *Sol. Stat. Commun.* **95**, 723 (1995).
- ¹⁸J. Shao, R. Winterhoff, A. Dornen, E. Baars, and J. Chu, *Phys. Rev. B* **68**, 165327 (2003).
- ¹⁹A. M. Mintairov, J. L. Merz, and A. S. Vlasov, *Phys. Rev. B* **67**, 205211 (2003).
- ²⁰U. Hakanson, T. Sass, M. K.-J. Johansson, M.-E. Pistol, and L. Samuelson, *Phys. Rev. B* **66**, 235308 (2002).
- ²¹A. Gocalinska, M. Manganaro, E. Pelucchi, and D. D. Vvedensky, *Phys. Rev. B* **86**, 165307 (2012).
- ²²O. Ambacher, J. Smart, J. R. Shealy, N. G. Weimann, K. Chu, M. Murphy, W. J. Schaff, and L. F. Eastman, *J. Appl. Phys.* **85**, 3222 (1999).
- ²³M. J. Gregor, P. G. Blome, and R. G. Ulbrich, *Appl. Phys. Lett.* **67**, 3572 (1995).
- ²⁴U. Kops, R. G. Ulbrich, M. Burkard, C. Geng, F. Scholz, and M. Schweizer, *Phys. Status Solidi A* **164**, 459 (1997).
- ²⁵S. Smith, H. M. Cheong, B. D. Fluegel, J. F. Geisz, J. M. Olson, L. L. Kazmerski, and A. Mascarenhas, *Appl. Phys. Lett.* **74**, 706 (1999).
- ²⁶U. Kops, P. G. Blome, M. Wenderoth, R. G. Ulbrich, C. Geng, and F. Scholz, *Phys. Rev. B* **61**, 1992 (2000).
- ²⁷S. Smith, A. Mascarenhas, and J. M. Olson, *Phys. Rev. B* **68**, 153202 (2003).